

Spherical and deformed structures in  $^{189}\text{Pb}$ A. M. Baxter,<sup>1,\*</sup> A. P. Byrne,<sup>1,2</sup> G. D. Dracoulis,<sup>2</sup> P. M. Davidson,<sup>2</sup> T. Kibédi,<sup>2</sup> R. V. F. Janssens,<sup>3</sup> M. P. Carpenter,<sup>3</sup> C. N. Davids,<sup>3</sup> T. L. Khoo,<sup>3</sup> and T. Lauritsen<sup>3</sup><sup>1</sup>*Department of Physics, Faculty of Science, Australian National University, Canberra ACT 0200, Australia*<sup>2</sup>*Department of Nuclear Physics, RSPHysSE, Australian National University, Canberra ACT 0200, Australia*<sup>3</sup>*Physics Division, Argonne National Laboratory, Argonne, Illinois 60439, USA*

(Received 2 January 2005; published 5 May 2005)

$\gamma$ -ray spectroscopy of high-spin states of the neutron-deficient nucleus  $^{189}\text{Pb}$  has been conducted with the  $^{158}\text{Gd}(^{36}\text{Ar},5n)$  and  $^{164}\text{Er}(^{29}\text{Si},4n)$  reactions. With the first of these, detection of evaporation residues and mass gating were used to unambiguously assign a number of prompt  $\gamma$ -ray transitions to  $^{189}\text{Pb}$ . With the second reaction and a pulsed beam, an isomer with a mean life of 32  $\mu\text{s}$  was found. Although inconclusive, the available evidence favors identification of the isomer with the  $\frac{33}{2}^+$  state of the  $\nu(i_{13/2})^{-3}$  configuration. The levels observed below the isomer can be identified with states involving three different structures: the neutron  $(i_{13/2})^{-3}$  multiplet in the spherical well; a prolate-deformed band involving mixed  $i_{13/2}$  neutron orbitals; and a state with the oblate  $\pi(2p-2h)_{0^+} \otimes \nu(i_{13/2})^{-1}$  configuration. The evidence for structures associated with different shapes is supported by the observation of  $E0$  components in some of the  $J^\pi \rightarrow J^\pi$  transitions linking them.

DOI: 10.1103/PhysRevC.71.054302

PACS number(s): 21.10.Re, 23.20.Lv, 27.70.+q, 21.10.Tg

## I. INTRODUCTION

Shape coexistence in the neutron-deficient, even-mass isotopes of lead is a well-established and much-studied phenomenon. The first indications of prolate-deformed, rotational bands at low excitation in these nuclei were found about a decade ago in the isotopes  $^{186}\text{Pb}$  [1,2] and  $^{188}\text{Pb}$  [1]. In both cases, the main feature of the yrast levels at low energy was a single band with rotationlike spacing for the third and higher excited levels. Its similarity to the well-established, yrast, prolate band observed in the corresponding isotones  $^{184}\text{Hg}$  [3,4] and  $^{186}\text{Hg}$  [3,5] was taken as evidence for prolate deformation, confirming early theoretical predictions [6–8] that a prolate minimum in the potential well for Pb nuclei should decrease in energy with decreasing neutron number  $N$ , relative to the spherical ground state, reaching a minimum near  $N = 104$ .

A subsequent study of the  $\alpha$  decay of  $^{190}\text{Po}$  [9] found evidence for two excited  $0^+$  states in  $^{186}\text{Pb}$  at 532 and 650 keV, and these have been associated with bandheads in prolate and oblate potential minima, respectively. In  $^{188}\text{Pb}$ , as well as the likely prolate yrast band, shape coexistence is revealed [10,11] through the presence of three isomers: an oblate  $11^-$  state with a  $\pi(\frac{9}{2}^- [505] \otimes \frac{13}{2}^+ [606])$  configuration; the  $12^+$  member of the  $\nu(i_{13/2})^{-2}$  multiplet in the spherical well; and an  $8^-$ ,  $\nu(\frac{7}{2}^- [514] \otimes \frac{9}{2}^+ [624])$ , two-quasineutron excitation at prolate deformation. There is also a good case [12] for triple shape coexistence in  $^{190}\text{Pb}$ : as well as the oblate  $11^-$  and  $12^+$  isomers, there is a candidate for the prolate band although it is located several hundred keV higher in excitation than in  $^{188}\text{Pb}$  and it is not yrast. The experimental evidence for coexisting spherical, oblate, and prolate structures in the even-mass, neutron-deficient lead isotopes has been supported by recent theoretical studies [13–16].

In the neutron-deficient, odd-mass lead isotopes, evidence for shape coexistence has been found mainly in radioactive decay studies. For example, strong  $E0$  components have been observed in transitions between certain states in  $^{195}\text{Pb}$  (Griffin *et al.* [17]) and  $^{197}\text{Pb}$  (Vanhorenbeeck *et al.* [18]) following  $\beta$  decay of the corresponding bismuth isotopes. These states have been identified with members of multiplets formed from weak coupling of an odd  $i_{13/2}$  neutron to spherical, or deformed-intruder,  $0^+$  and  $2^+$  states in the neighboring even-mass core. Studies of  $\alpha$  decay of polonium isotopes have yielded similar results. Andreyev *et al.* [19] studied fine structure in the  $\alpha$  decay of  $^{191}\text{Po}$  and deduced several excited states in  $^{187}\text{Pb}$ . From a combination of experimental limits on the spins and parities and expectations from theoretical calculations, they speculated that one of them, at 494-keV excitation relative to the  $\frac{13}{2}^+$  isomer, is the bandhead of an oblate intruder band and another, at 472 keV, is the bandhead of a prolate  $\frac{9}{2}^+$  [624] band. In similar  $\alpha$ -decay fine-structure measurements Van de Vel *et al.* [20] identified levels in  $^{189-193}\text{Pb}$  that they interpreted as oblate intruder states. In particular, they found two such levels in  $^{189}\text{Pb}$ : a  $\frac{3}{2}^-$  state 549 keV above the ground state and a  $\frac{13}{2}^+$  state 637 keV above the  $\frac{13}{2}^+$  isomer.

In-beam studies have so far yielded little additional evidence for shape coexistence in the very-neutron-deficient odd-mass isotopes. While this is no doubt due largely to the lack of data on odd-mass isotopes with  $A < 191$ , it may be more difficult, because of their greater complexity, to identify well-deformed prolate structures in the odd-mass isotopes than in their even-mass neighbors. In  $^{193}\text{Pb}$ , the properties of high-spin states have been studied by several groups [21–26]. However, apart from superdeformed bands, the only evidence for significant deformation is in states, such as a  $J^\pi = \frac{29}{2}^-$  isomer, that are attributed to the coupling of one or three rotation-aligned quasineutrons to the oblate  $11^-$ , two-quasiproton excitation in the neighboring, even- $A$  isotope. The level sequences built on these states are dipole

\*Electronic address: a.baxter@anu.edu.au

bands which have been associated with the so-called shears mechanism (see, e.g., [27]) rather than with simple rotation. Level schemes for  $^{191}\text{Pb}$  have been presented by Fotiades *et al.* [28] and Lagrange *et al.* [29] and have been largely confirmed and extended by recent work in this laboratory [30]. The observed high-spin structures in  $^{191}\text{Pb}$  are similar to those seen in  $^{193}\text{Pb}$  and heavier, odd-mass isotopes, with little evidence of collective behavior. In  $^{187}\text{Pb}$ , a single cascade of  $\gamma$  rays has been observed [31], terminating at the low-lying  $\frac{13}{2}^+$  isomer; systematic trends in heavier Pb isotopes suggest that the levels concerned arise from the weak coupling of an  $i_{13/2}$  neutron hole to the yrast states in the spherical potential minimum of the neighboring even- $A$  core.

The principal aim of the present work was to investigate whether  $^{189}\text{Pb}$  exhibits evidence for shape coexistence like that seen in  $^{186}\text{Pb}$ ,  $^{188}\text{Pb}$ , and  $^{190}\text{Pb}$ . The key indication would be competition from well-defined prolate structures, such as those seen in the isotope  $^{187}\text{Hg}$  [32], with the spherical and weakly deformed oblate states that are ubiquitous in the heavier odd-mass isotopes. The study of very neutron-deficient nuclei such as  $^{189}\text{Pb}$  by fusion-evaporation reactions is experimentally challenging owing to the severe competition from fission and the fragmented nature of the decays. To help overcome these difficulties, a variety of techniques was employed, including detection of prompt decays in coincidence with evaporation residues to give definitive mass identification and, in separate experiments, pulsed-beam measurements that led to identification of a long-lived isomer and excited states in its decay paths.

## II. EXPERIMENTAL METHODS

For the study of prompt decays of  $^{189}\text{Pb}$ , excited levels were populated by bombarding a  $^{158}\text{Gd}$  target with 178-MeV  $^{36}\text{Ar}$  ions from the ATLAS superconducting, linear accelerator at the Argonne National Laboratory. The target was a self-supporting metallic foil, 0.43-mg/cm<sup>2</sup> thick, enriched to 92.9% in  $^{158}\text{Gd}$ . The Argonne fragment mass analyzer (FMA) was set at 0° to the beam to accept evaporation residues recoiling from the target, and  $\gamma$  radiation was detected by 10 Compton-suppressed germanium detectors, of the Argonne–Notre Dame bismuth germanate  $\gamma$ -ray facility, placed around the target.

The FMA (Davids *et al.* [33]) is a recoil mass spectrometer that produces dispersion in the mass/charge ratio of the reaction products. Recoiling ions that reached the focal plane were detected by a parallel-grid avalanche counter (PGAC), of 15 by 5 cm active area, which produced energy loss ( $\Delta E$ ) and focal-plane-position signals. Other experimental details concerning the FMA, as it was used in this experiment, may be found in Ref. [2]. Singles  $\gamma$ -ray spectra and  $\gamma$ - $\gamma$ -coincidence data were acquired, gated in both cases by recoils.

For the study of isomers and their decays, high-spin states in  $^{189}\text{Pb}$  were populated by bombarding a target of  $^{164}\text{Er}$  with 140-MeV  $^{29}\text{Si}$  beams from the 14UD Pelletron accelerator at the Australian National University. The target was a self-supporting metallic foil, 2.5-mg/cm<sup>2</sup> thick, isotopically enriched to 73.6% in  $^{164}\text{Er}$ , with a 4-mg/cm<sup>2</sup> layer of lead evaporated on the back to stop the recoiling nuclei. The main

isotopic contaminant in the target was 15.0% of  $^{166}\text{Er}$ , the presence of which led to significant population of high-spin states in  $^{190}\text{Pb}$ ,  $^{191}\text{Pb}$ , and  $^{192}\text{Pb}$ .  $\gamma$ -rays were detected in the six Compton-suppressed germanium detectors and two planar low energy photon spectrometer (LEPS) detectors of the CAESAR array.

After an initial exploration of the  $\mu\text{s}$  region using a variety of chopped beam conditions, lifetimes of longer-lived isomers were measured with the  $^{29}\text{Si}$  beam pulsed with on/off periods of 32 and 160  $\mu\text{s}$ , respectively. The time of detection of a  $\gamma$  ray in any of the detectors was measured with a 4-MHz digital clock, which was reset in synchronization with the pulsing period. To establish the decay scheme below long-lived isomers, the beam pulsing periods were changed to 2.1  $\mu\text{s}$  on and 17.1  $\mu\text{s}$  off, and  $\gamma$ - $\gamma$ -time coincidence data were acquired only during the beam-off period. Time relationships between  $\gamma$  rays were determined from fast time-to-digital converters (TDCs) associated with each detector.

Additional data on  $^{189}\text{Pb}$  have recently become available in a study [11] of  $^{188}\text{Pb}$  in which  $^{189}\text{Pb}$  was produced as a contaminant. These data provided independent confirmation of some of the present results.

## III. DATA ANALYSIS AND RESULTS

The level scheme of  $^{189}\text{Pb}$  deduced in this work is shown in Fig. 1; it incorporates the results from both the in-beam and out-of-beam measurements. Transition energies, relative intensities, and level assignments are also listed in Table I.

### A. Mass-gated recoil- $\gamma$ and recoil- $\gamma$ - $\gamma$ data

The mass spectrum of recoil ions detected at the focal plane of the FMA is presented in Fig. 2. The electric and magnetic fields of the FMA were set so that the two most abundant charge states ( $Q = 18$  and 19) of mass-189 ions both fitted within the acceptance aperture of the PGAC at the focal plane.

The spectrum in Fig. 2 was obtained by projecting onto the position axis a matrix of position in the PGAC vs  $E_\gamma$  corrected for Doppler shifts. It was required that the transit time of the ions through the FMA and the  $\Delta E$  pulse from the PGAC both corresponded to evaporation residues; events involving fission or Coulomb excitation were thereby rejected. The mass resolving power  $M/\Delta M$  in the spectrum (Fig. 2) is approximately 250 and is sufficient to distinguish peaks corresponding to adjacent mass values.

The spectrum shown in Fig. 3 is a sum of projections on the  $E_\gamma$  axis of the position vs  $E_\gamma$  matrix, with gates on the two mass-189 peaks in the position spectrum (Fig. 2). Most of the strong peaks in the mass-gated  $\gamma$ -ray spectrum can be identified with known transitions in  $^{189}\text{Tl}$  [34] and with x rays from lead, thallium, and gadolinium. (The Gd x rays presumably arise from coincidences with beam particles scattered through the FMA and from random coincidences.) As will be discussed below, several of the remaining peaks can be unambiguously assigned to  $^{189}\text{Pb}$  on the evidence of their coincidences with one another and with lead x rays.

Figure 4 shows a composite spectrum of  $\gamma$  rays attributed to  $^{189}\text{Pb}$ , obtained from the mass-gated  $\gamma$ - $\gamma$ -coincidence data.

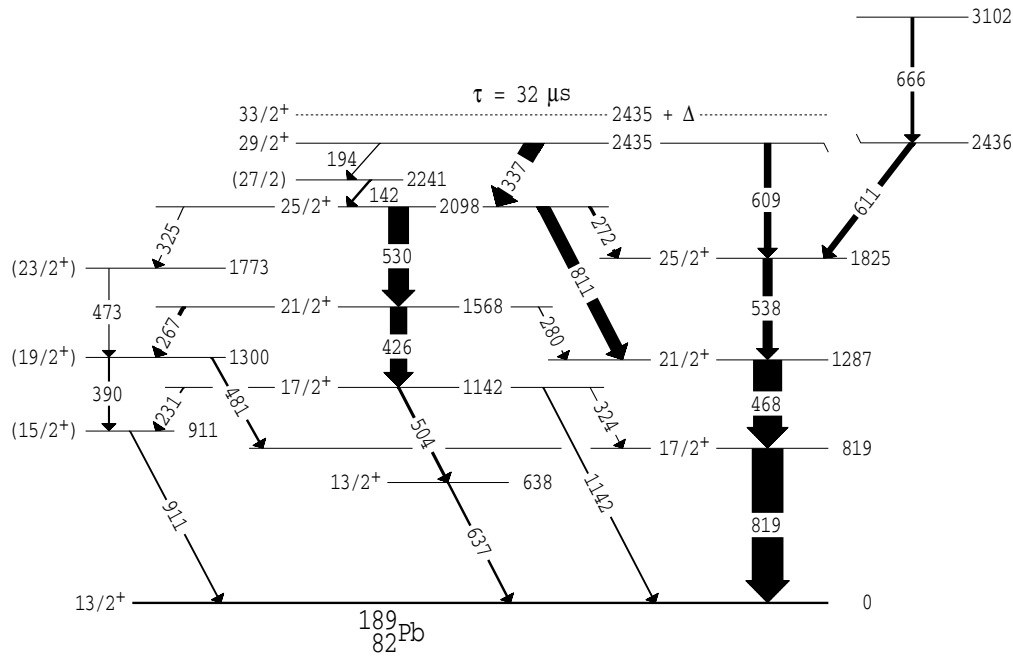


FIG. 1. Energy level and decay scheme of  $^{189}\text{Pb}$  determined in the present work. Excitation energies are relative to the long-lived  $\frac{13}{2}^+$  isomer. The widths of the arrows indicate the relative  $\gamma$ -ray intensities. As explained in the text, many of the spin and parity assignments are based on complex arguments and should be regarded as tentative.

The coincident Pb x rays identify the atomic number of the emitting nuclei. The 468-, 538-, 611- and 819-keV lines are all in coincidence with one another and therefore form a cascade as shown in the level scheme (Fig. 1). The 611-keV peak in the composite spectrum (Fig. 4) is broader than its neighbors; however, this broadening appears only in the spectrum gated by 819-keV  $\gamma$  rays. There is either a second prompt transition with energy near 611 keV that feeds the 819-keV level, or a contaminant from another nuclide in the 819-keV gate. The 811-keV line is seen weakly but clearly in the mass-gated spectra in coincidence with the 468- and 819-keV  $\gamma$  rays, while the spectrum in coincidence with 811-keV  $\gamma$  rays shows only lines at 142, 468, and 819 keV as well as Pb x rays. The 666-keV line is seen weakly in the mass-gated spectra in coincidence with 819-, 468-, and 538-keV  $\gamma$  rays and very weakly in the 611-keV gate. The ordering of the 611- and 666-keV transitions is based on their relative intensities. The 530-426-1142-keV and 390-911-keV sequences shown in Fig. 1 also appeared very weakly in the mass-gated  $\gamma$ - $\gamma$  data.

Two prominent lines, at 264 and 854 keV, that were in coincidence with mass-189 recoils (Fig. 3) could not definitely be assigned to a particular nuclide. The 264-keV  $\gamma$  rays were found, in the recoil- $\gamma$ - $\gamma$  data, to be in coincidence with weak Pb x rays and with lines at 279, 394, and 602 keV. However, they showed no coincidence relationship with any of the  $^{189}\text{Pb}$   $\gamma$  rays identified in the present work. These  $\gamma$  rays may be prompt transitions feeding the 32- $\mu\text{s}$  isomer identified in the delayed- $\gamma$  data. (Transitions with energies near 264 keV have been reported in  $^{189}\text{Au}$  and  $^{190}\text{Hg}$ ; however, the coincidence relationships expected in these cases do not

correspond to those seen here.) The 854-keV peak, seen in the composite spectrum (Fig. 4), appears only in the coincidence gate on the 468-keV line. In the spectrum gated by 854-keV  $\gamma$  rays, a 470-keV line is seen close to but definitely higher in energy than the 468-keV transition in  $^{189}\text{Pb}$ . Coincident x rays, although weak, suggest the 854-keV  $\gamma$  rays are from Tl; however, no such transition in  $^{189}\text{Tl}$  has been reported in previous work on this nucleus [34]. An 853.4 keV line has been reported in  $^{189}\text{Hg}$ , but no correlation with a 470-keV line was observed.

The angular distributions of the  $^{189}\text{Pb}$   $\gamma$  rays in the recoil- $\gamma$  data were isotropic within statistical uncertainties, presumably because of vacuum deorientation, so it was not possible to obtain any information on spins from these data. On the basis of systematic trends, it is assumed that the lowest level shown in Fig. 1 is the low-lying  $\frac{13}{2}^+$  isomer observed (e.g., Ref. [21]) in the heavier, odd-mass, lead isotopes and, also from these trends, its excitation energy is expected to be about 100 keV. However, since this excitation is not known, the excitation energies of levels in Fig. 1 and the following discussion are all given relative to this  $\frac{13}{2}^+$  isomer. The spins and parities assigned to higher levels in Fig. 1 are based on the arguments presented below.

### B. Search for isomers in $^{189}\text{Pb}$

As described earlier, a search for isomers in  $^{189}\text{Pb}$  was conducted by bombarding a lead-backed,  $^{164}\text{Er}$  target with a pulsed beam of 140-MeV  $^{29}\text{Si}$  ions. In the spectra of  $\gamma$  rays emitted between beam pulses, the 468-, 811- and

TABLE I. Energies and relative intensities of transitions assigned to  $^{189}\text{Pb}$  with excitation energies and assigned spins and parities for the corresponding initial and final states. Excitation energies are relative to the long-lived  $\frac{13}{2}^+$  isomer.

$E_\gamma$ (keV)	$I_\gamma$ in-beam	$I_\gamma$ out-of-beam	$E_i$ (keV)	$E_f$ (keV)	$J_i^\pi$	$J_f^\pi$
142.4(2)	35(12)	35(5)	2240.5	2097.9	$(\frac{27}{2})$	$\frac{25}{2}^+$
193.9(3)		22(5)	2434.6	2240.5	$\frac{29}{2}^+$	$(\frac{27}{2})$
230.9(2)		31(12)	1141.7	910.7	$\frac{17}{2}^+$	$(\frac{15}{2}^+)$
267.4(3)		68(16)	1567.8	1300.3	$\frac{21}{2}^+$	$(\frac{19}{2}^+)$
272.4(2)		55(10)	2097.9	1825.4	$\frac{25}{2}^+$	$\frac{25}{2}^+$
279.7(2)		23(5)	1567.8	1287.2	$\frac{21}{2}^+$	$\frac{21}{2}^+$
323.5(3)		18(6)	1141.7	818.8	$\frac{17}{2}^+$	$\frac{17}{2}^+$
325.0(5)		20(10)	2097.9	1773	$\frac{25}{2}^+$	$(\frac{23}{2}^+)$
336.7(1)		290(30)	2434.6	2097.9	$\frac{29}{2}^+$	$\frac{25}{2}^+$
389.7(2)	$\sim 40$	34(10)	1300.3	910.7	$(\frac{19}{2}^+)$	$(\frac{15}{2}^+)$
425.9(1)	$\sim 40$	275(55)	1567.8	1141.7	$\frac{21}{2}^+$	$\frac{17}{2}^+$
468.4(1)	375(40)	395(20)	1287.2	818.8	$\frac{21}{2}^+$	$\frac{17}{2}^+$
473.0(5)		20(10)	1773	1300.3	$(\frac{23}{2}^+)$	$(\frac{19}{2}^+)$
481.2(2)		40(15)	1300.3	818.8	$(\frac{19}{2}^+)$	$\frac{17}{2}^+$
503.8(3)		50(11)	1141.7	637.7	$\frac{17}{2}^+$	$\frac{13}{2}^+$
530.3(1)	$\sim 40$	330(70)	2097.9	1567.8	$\frac{25}{2}^+$	$\frac{21}{2}^+$
538.2(1)	120(12)	160(15)	1825.4	1287.2	$\frac{25}{2}^+$	$\frac{21}{2}^+$
609.3(3)		55(10)	2434.6	1825.4	$\frac{29}{2}^+$	$\frac{25}{2}^+$
611.0(4)	100(20)		2436.4	1825.4		$\frac{25}{2}^+$
637.4(3)	100(10)	40(15)	637.7	0	$\frac{13}{2}^+$	$\frac{13}{2}^+$
666.0(5)	60(20)		3102.4	2436.4		
810.8(2)	45(10)	200(12)	2097.9	1287.2	$\frac{25}{2}^+$	$\frac{21}{2}^+$
818.8(1)	500	500	818.8	0	$\frac{17}{2}^+$	$\frac{13}{2}^+$
910.6(3)	110(11)	60(10)	910.7	0	$(\frac{15}{2}^+)$	$\frac{13}{2}^+$
1142.1(6)	100(30)	55(10)	1141.7	0	$\frac{17}{2}^+$	$\frac{13}{2}^+$

819-keV  $\gamma$ -ray lines were all found to exhibit a mean life of approximately  $30 \mu\text{s}$ ; the time spectra corresponding to the 468- and 819-keV transitions, projected from the  $\gamma$ -ray energy-time matrix, are presented in Fig. 5. (Throughout the present work lifetimes of states are given as mean lives rather than half-lives.) These decay curves could be fitted with a single exponential decay function and a flat component independent of time over the range concerned. Projections of  $\gamma$ -ray spectra corresponding to consecutive bins on the time axis showed that the lines associated with the flat component had energies slightly different from those of the exponentially decaying component. It is therefore likely that the flat component arises from very long-lived products of  $\beta$  decay, justifying the inclusion of a constant component in the fit, although its magnitude is uncertain. The mean lives deduced from best fits to the data were  $34 \pm 4$  and  $30 \pm 3 \mu\text{s}$  for the 468- and 819-keV transitions, respectively; these were obtained while allowing the constant component to be adjusted in the fit. If the

constant component is set to zero, the lifetimes obtained are 50 and  $45 \mu\text{s}$ , respectively. From these considerations, the value adopted for the mean life from these fits is  $32_{-2}^{+10} \mu\text{s}$ . Because of contamination of the  $\gamma$ -ray gates, it was very difficult to obtain satisfactory time spectra for other  $^{189}\text{Pb}$  transitions. The 811-keV line also showed a lifetime of approximately  $30 \mu\text{s}$ , but there was a large constant component, presumably from contamination with radiation from  $\beta$ -decay products. The other strong lines were contaminated by transitions in other nuclei, notably  $^{190}\text{Pb}$ .

The delayed- $\gamma$ - $\gamma$ -time coincidence data were sorted to measure time relationships between members of the stronger cascades in the decay scheme. No evidence was found for significant lifetimes for any of the intermediate levels and, in particular, the following upper limits on the mean lives of certain of these levels were obtained from TDC differences: 1142-keV level,  $<10 \text{ ns}$ ; 1287,  $<3 \text{ ns}$ ; 1568,  $<4 \text{ ns}$ ; and 2098,  $<3 \text{ ns}$ .

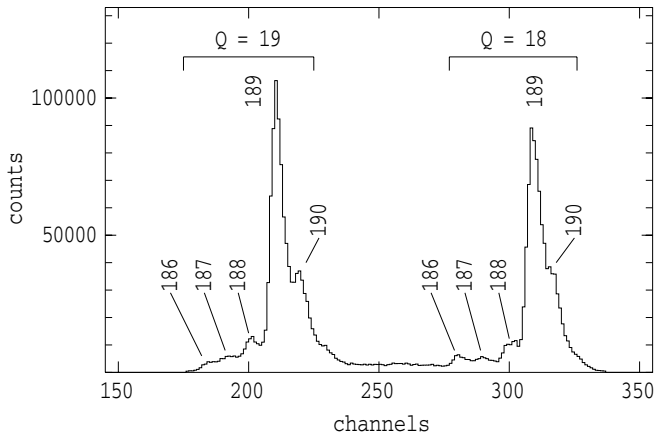


FIG. 2. Mass spectrum from a projection onto the position axis of the PGAC position vs  $E_\gamma$  matrix obtained with the  $^{36}\text{Ar} + ^{158}\text{Gd}$  reaction. Peaks are labeled by the mass number of the recoiling ions and fall into two groups corresponding to charge states  $Q = 18$  and  $19$ .

**C. Decay of the 32- $\mu\text{s}$  isomer**

The decay scheme below the 32- $\mu\text{s}$  isomer in  $^{189}\text{Pb}$  was deduced from the  $\gamma$ - $\gamma$ -coincidence data acquired between beam pulses separated by 17.1  $\mu\text{s}$  (the delayed- $\gamma$ - $\gamma$  data). A  $4096 \times 4096$  channel matrix was constructed from those events from the six Compton-suppressed germanium detectors in which the two  $\gamma$ -rays were detected within  $\pm 120$  ns of each other. Background-subtracted spectra, with gates on individual  $\gamma$ -ray lines, were projected from this matrix and used to determine the coincidence relationships between transitions. Examples of these spectra are shown in Fig. 6, and the level scheme deduced from the delayed- $\gamma$ - $\gamma$  and lifetime data, as well as the prompt, mass-gated,  $\gamma$ - $\gamma$  data discussed earlier, is given in Fig. 1. The ordering of transitions is determined by coincidence relationships and relative intensities.

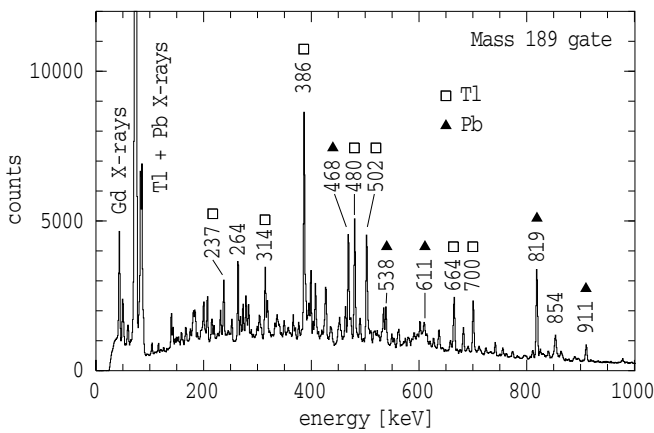


FIG. 3. Part of the  $\gamma$ -ray spectrum gated by the two mass-189 peaks in the PGAC position spectrum obtained with the  $^{36}\text{Ar} + ^{158}\text{Gd}$  reaction. Most of the more prominent peaks are labeled by their energies and the nucleus to which they are assigned; peaks labeled by energy only are discussed in the text.

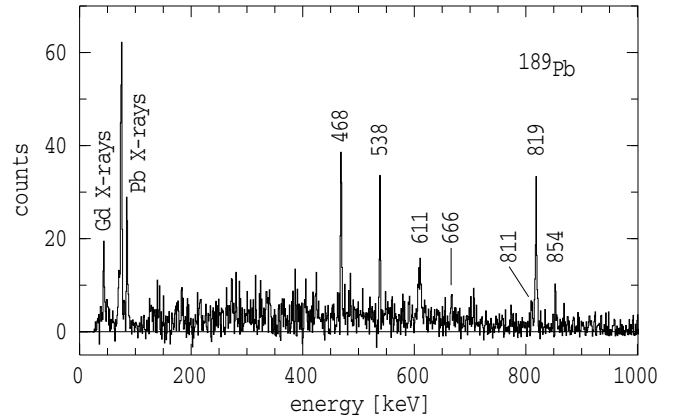


FIG. 4. Sum of projections from the recoil- $\gamma$ - $\gamma$  coincidence data with gates on the 468-, 538-, 611- and 819-keV lines.

In the absence of angular distribution information, assignments of level spins and parities were based on systematic trends in neighboring isotopes and isotones, total internal conversion coefficients deduced from intensity balances below the isomer, and reasonable limits on transition strengths of certain multipolarities deduced from the lifetime of the isomer and the measured upper limits on the lifetimes of some other levels.

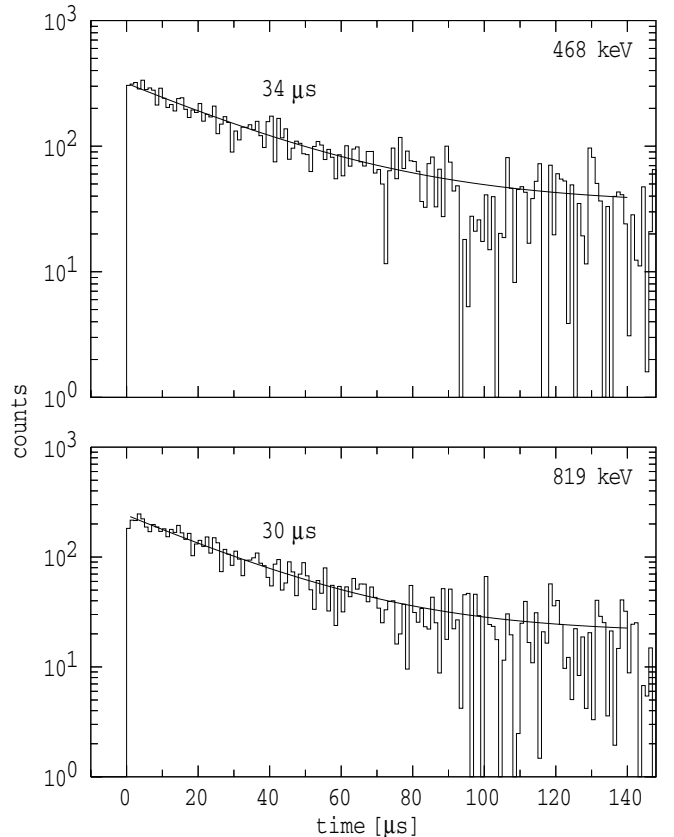


FIG. 5. Spectra showing the time of detection relative to the beam pulse of the 468- and 819-keV transitions in  $^{189}\text{Pb}$ . In each case, the fit to the spectrum is shown together with the deduced mean life.

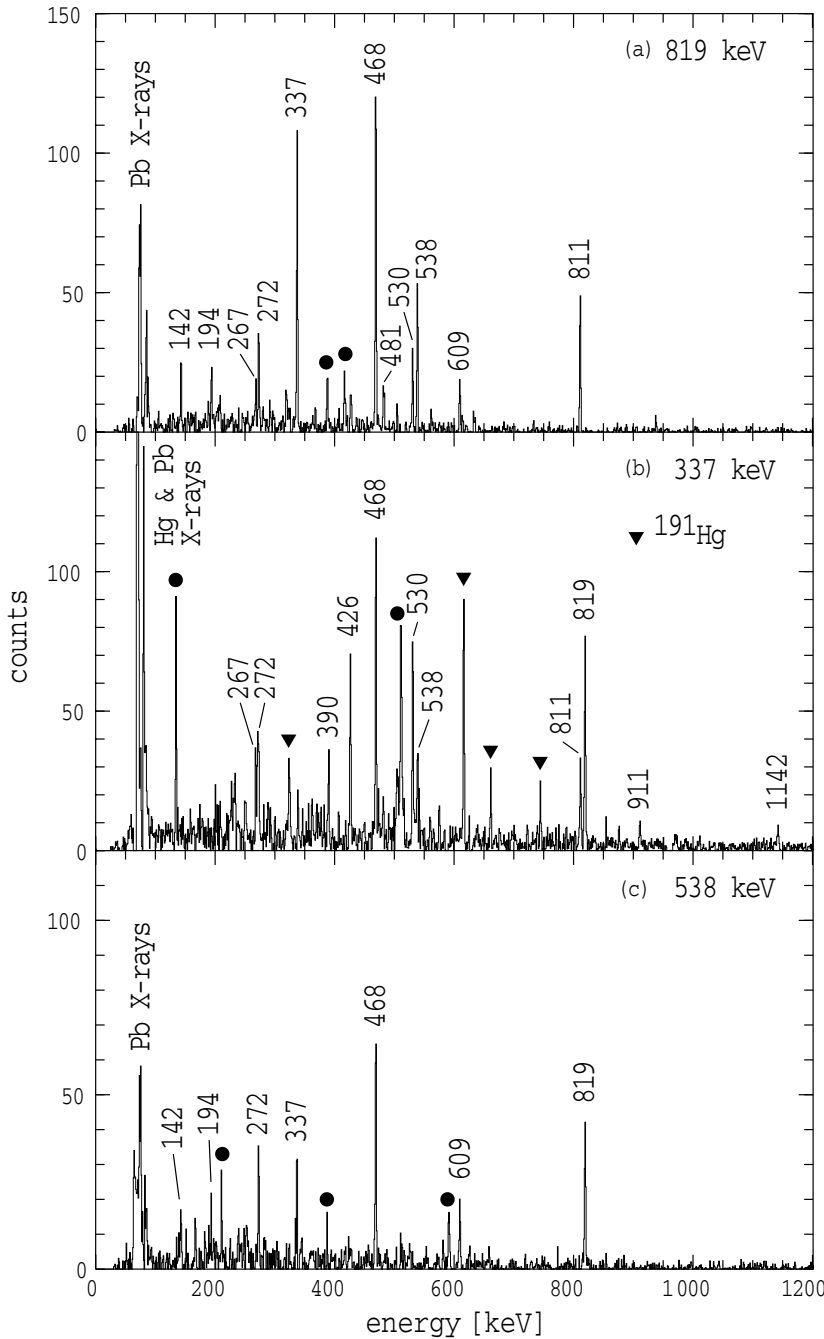


FIG. 6. Spectra of  $\gamma$  rays in coincidence with the 819-, 337-, and 538-keV transitions in  $^{189}\text{Pb}$ . The spectra are from the delayed- $\gamma$ - $\gamma$  data. Peaks attributed to  $^{189}\text{Pb}$  are labeled by their energies in keV and others by symbols. Those marked with filled circles could not be identified, but are probably associated with the products of  $\beta$  decay.

In Fig. 7, the excitation energies of the  $^{189}\text{Pb}$  levels at 819, 1287, 1825, and 2435 keV are compared with those of the yrast  $\frac{17}{2}^+$ ,  $\frac{21}{2}^+$ ,  $\frac{25}{2}^+$ ,  $\frac{29}{2}^+$ , and  $\frac{33}{2}^+$  levels in the odd- $A$  isotopes  $^{191-199}\text{Pb}$ . Except in the case of  $^{199}\text{Pb}$ , the levels are connected by a cascade of  $E2$  transitions. For  $^{191,193,195,197}\text{Pb}$ , these levels may be identified with states in the spherical well involving predominantly the  $(i_{13/2})^{-3}$  multiplet, although the lower-spin members probably have significant contributions from other neutron configurations. Extrapolation to  $^{189}\text{Pb}$  of the smooth trends of excitation energies for these levels suggests assignments of  $J^\pi = \frac{17}{2}^+$ ,  $\frac{21}{2}^+$ , and  $\frac{25}{2}^+$  to the  $^{189}\text{Pb}$

levels at 819, 1287, and 1825 keV, respectively. The 2435-keV level is considered later in more detail.

An attempt was made to measure directly internal conversion coefficients for some of the stronger transitions, but this was not successful because of the small cross section for producing  $^{189}\text{Pb}$  and the complexity of the singles spectra for electrons and  $\gamma$  rays. However, it was possible to infer total conversion coefficients for some transitions from intensity balance considerations in some cascades below the isomer. The results of significance for determining spins and parities are summarized in Table II. The  $\alpha_T$  values given in Table II were extracted from gated cascades chosen to give the cleanest

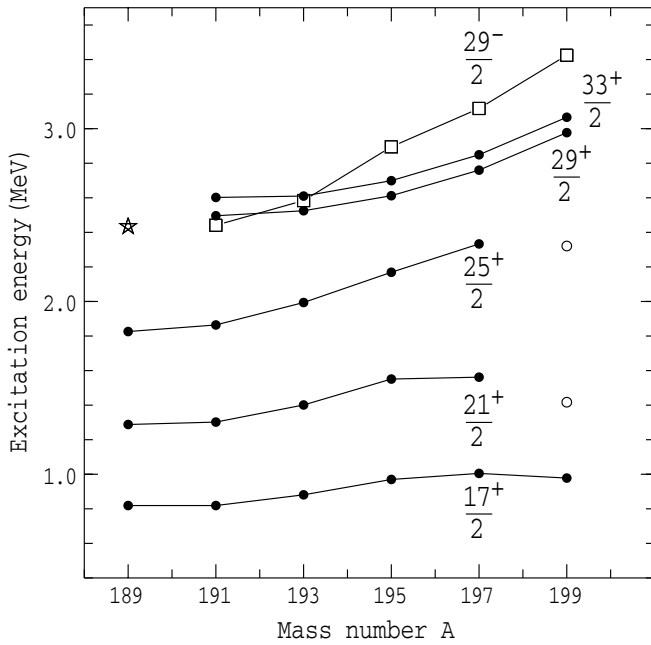


FIG. 7. Variation with mass number  $A$  of the excitation energies relative to the long-lived  $\frac{13}{2}^+$  isomer of some yrast levels in the neutron-deficient, odd-mass, lead isotopes. The star symbol represents the 2435-keV level in  $^{189}\text{Pb}$ . The data are from this work ( $^{189}\text{Pb}$ ), [29,30]( $^{191}\text{Pb}$ ), [24]( $^{193}\text{Pb}$ ), [35]( $^{195}\text{Pb}$ ), [36]( $^{197}\text{Pb}$ ), and [37]( $^{199}\text{Pb}$ ).

spectra and may differ slightly from those implied by the intensities in Table I.

Application of the requirements of intensity balance to the 272-keV transition depopulating the 2098-keV level leads to a total conversion coefficient of 1.50(20). This significantly exceeds the theoretical values  $\alpha_T(M1) = 0.56$  and  $\alpha_T(E2) = 0.16$  [38], implying an  $E0$  component and hence a  $J^\pi \rightarrow J^\pi$  transition. Adopting the assignment, from systematics, of  $J^\pi = \frac{25}{2}^+$  to the 1825-keV level, we conclude that the 2098-keV level also has  $J^\pi = \frac{25}{2}^+$ . Similarly the total conversion coefficient for the 324-keV transition is found, from intensity balance, to be 1.5(5). Comparison of this with the theoretical conversion coefficients [38] for  $M1$  and  $E2$  multiplicities (0.35 and 0.092, respectively) strongly suggests that the 324-keV transition has a significant  $E0$  component, and we therefore assign  $J^\pi = \frac{17}{2}^+$  to the 1142-keV level.

Very weak 504- and 637-keV  $\gamma$  rays were observed in the 426- and 530-keV gates of the delayed- $\gamma$ - $\gamma$  data. The 637-keV

TABLE II. Total internal conversion coefficients  $\alpha_T$  for likely  $J^\pi \rightarrow J^\pi$  transitions in  $^{189}\text{Pb}$  determined from intensity balances in cascades below the 32- $\mu\text{s}$  isomer.

$E_\gamma$ (keV)	$E_i$ (keV)	$E_f$ (keV)	$J_i^\pi$	$J_f^\pi$	$\alpha_T$
272	2098	1825	$\frac{25}{2}^+$	$\frac{25}{2}^+$	1.50(20)
324	1142	819	$\frac{17}{2}^+$	$\frac{17}{2}^+$	1.5(5)
637	638	0	$\frac{13}{2}^+$	$\frac{13}{2}^+$	0.40(35)

line is identified with a transition of the same energy observed by Van de Vel *et al.* [20] following the  $\alpha$  decay of  $^{193}\text{Po}$ . From  $\alpha$ -particle energies and  $\alpha$ - $\gamma$  coincidences, they placed this transition as the decay to the long-lived  $\frac{13}{2}^+$  isomer in  $^{189}\text{Pb}$  of an excited state, 637 keV above the isomer. They also measured the total conversion coefficient for this transition as  $\alpha_T = 1.1(4)$ , indicating a significant  $E0$  contribution to the 637-keV transition, and hence that the 637-keV level also has  $J^\pi = \frac{13}{2}^+$ . We find, from intensity balance,  $\alpha_T(637) = 0.40(35)$ , consistent with the conclusion of Van de Vel *et al.* [20] that the transition has an  $E0$  component. A very weak 637-keV  $\gamma$ -ray line is also observed in the prompt recoil- $\gamma$ - $\gamma$  data in coincidence with 426-keV  $\gamma$  rays.

From coincidence relationships and energy sums, we place the observed 504-keV  $\gamma$  ray as a transition between the 1142- and 638-keV levels. The upper limits on the lifetimes of the 1568- and 2098-keV levels and the requirements of reasonable transition strengths limit the possible multiplicities of the 530- and 426-keV transitions to  $E1$ ,  $M1$ , or  $E2$ . From these results and the assignments of  $\frac{25}{2}^+$  and  $\frac{17}{2}^+$  to the 2098- and 1142-keV levels, respectively, we deduce that the 530- and 426-keV transitions both have  $E2$  multiplicity and hence assign  $J^\pi = \frac{21}{2}^+$  to the 1568-keV level.

A third decay path from the 2098-keV level to the  $\frac{13}{2}^+$  isomer occurs via the levels (see Fig. 1) at 1773, 1300, and 911 keV. The transitions involved are weak and, in the case of the 325- and 473-keV lines, only slightly above the sensitivity limits of the present experiment. Their locations in the scheme are confirmed by a recent experiment [11], although in neither case could the ordering of the 325- and 473-keV transitions be determined. The order chosen is consistent with the 1773-keV level being a member of a rotational band as discussed below.

The part of the level scheme of  $^{189}\text{Pb}$  involving the levels at 911-, 1300-, and 1773-keV excitation and transitions between these and other levels are compared in Fig. 8 with part of a rotational band in the isotope  $^{187}\text{Hg}$ , reported by Hannachi *et al.* [32] and identified by them with the neutron  $\frac{9}{2}^+$  [624] configuration at prolate deformation. Based on the similarities of the two and the following arguments, we tentatively assign  $J^\pi = \frac{15}{2}^+$ ,  $\frac{19}{2}^+$ , and  $\frac{23}{2}^+$  to the 911-, 1300-, and 1773-keV levels, respectively. In the partial level schemes in Fig. 8, the excitation energies given are values relative to the yrast  $\frac{13}{2}^+$  state in each case. (In  $^{187}\text{Hg}$  the yrast  $\frac{13}{2}^+$  state is the ground state.) However, to aid comparison, the two schemes are aligned in the diagram so that the  $\frac{17}{2}^+$  states are at the same horizontal level.

In  $^{189}\text{Pb}$ , the level spacings correspond reasonably well to their putative counterparts in  $^{187}\text{Hg}$ . The agreement between the sequences with signature  $\alpha = -\frac{1}{2}$  is better than for the  $\alpha = +\frac{1}{2}$  sequences; this may well be due to perturbation of the  $\alpha = +\frac{1}{2}$  levels by mixing with the spherical states in the case of  $^{189}\text{Pb}$  and with the ground state band in  $^{187}\text{Hg}$ .

The cascade/crossover branching ratios,

$$\lambda = \frac{I_\gamma(\Delta I = 2)}{I_\gamma(\Delta I = 1)},$$

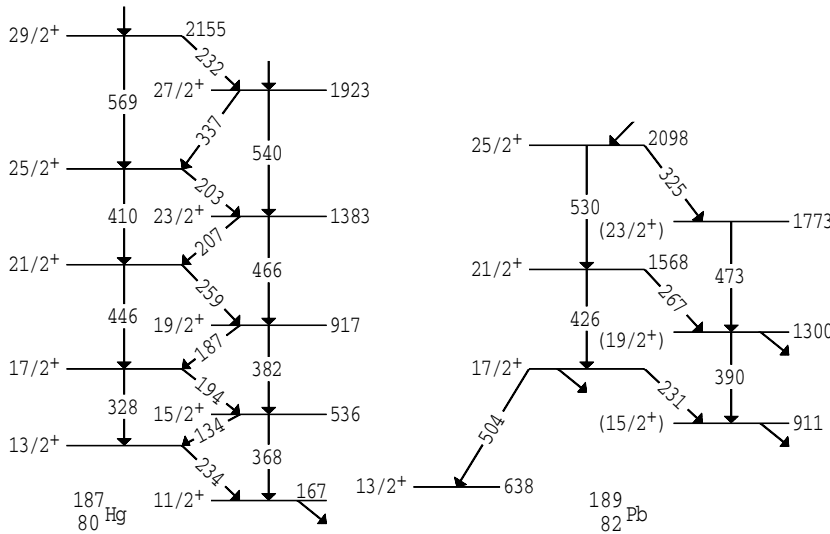


FIG. 8. Partial level schemes of the isotones  $^{187}\text{Hg}$  and  $^{189}\text{Pb}$ .

which depend upon the structure of the bands, can be compared for two cases, the  $\frac{21}{2}^+$  and  $\frac{25}{2}^+$  levels. In  $^{187}\text{Hg}$ , Hannachi *et al.* [32] obtain  $\lambda(\frac{21}{2}^+) = 11(4)$  and  $\lambda(\frac{25}{2}^+) = 4.5(23)$ . If one assumes that the values of  $g_K - g_R$  and the intrinsic quadrupole moment  $Q_0$  for the bands are the same, the rotational model predicts  $\lambda(\frac{21}{2}^+) = 7(4)$  and  $\lambda(\frac{25}{2}^+) = 4.2(23)$  for the branching ratios in  $^{189}\text{Pb}$ . The measured values (from the data in Table I) are  $\lambda(\frac{21}{2}^+) = 4.0(12)$  and  $\lambda(\frac{25}{2}^+) = 18(10)$ , which are roughly consistent with the predictions, although the errors are large. A similar calculation for the  $\frac{19}{2}^+$  and  $\frac{23}{2}^+$  levels in  $^{189}\text{Pb}$  predicts  $\lambda = 17(8)$  and  $11(4)$ , respectively. If the values in  $^{189}\text{Pb}$  are in fact of this magnitude, transitions between the  $(\frac{23}{2}^+)$  and  $(\frac{21}{2}^+)$  levels and between the  $(\frac{19}{2}^+)$  and  $(\frac{17}{2}^+)$  levels would be undetectable at the sensitivity of the current experiment. This would account for the failure to observe them.

No transition is observed from the  $\frac{17}{2}^+$  level at 1142 keV in  $^{189}\text{Pb}$  to a possible  $\frac{13}{2}^+$  member of the same band. If such a state exists, simple comparison with  $^{187}\text{Hg}$  (Fig. 8) suggests that, in the absence of mixing, it would lie at about 780-keV excitation. A transition to this state from the  $\frac{17}{2}^+$  level at 1142 keV may not compete sufficiently well with alternative transitions to the lower-lying  $\frac{13}{2}^+$  state at 638 keV or the spherical  $\frac{13}{2}^+$  isomer.

#### D. Spin and parity of the 2435-keV level

The 2435-keV level in  $^{189}\text{Pb}$  is the highest-lying level seen in the delayed- $\gamma$  data, which suggests it may be isomeric, and its principal decays are to  $\frac{25}{2}^+$  levels at 1825 and 2098 keV. Weak 142- and 194-keV lines are placed in cascade, in parallel with the 337-keV transition, between the 2435- and 2098-keV levels. Their ordering is determined by the observation of the 142-keV line, but not the 194-keV line, in the prompt decay data. The systematics shown in Fig. 7 suggest two candidates for the source of the 32- $\mu\text{s}$  lifetime observed in  $^{189}\text{Pb}$ : either a  $\frac{33}{2}^+$  state that would be the highest-spin member of the

neutron  $(i_{13/2})^{-3}$  multiplet, or a  $\frac{29}{2}^-$  level analogous to the one which is isomeric in  $^{191,193}\text{Pb}$ , although not in the higher-mass isotopes.

If the 2435-keV level is itself the 32- $\mu\text{s}$  isomer and has  $J^\pi = \frac{29}{2}^-$ , its principal decays (337 and 609 keV) would have to be of  $M2/E3$  multipolarity and the 142- and 194-keV lines would probably have  $E1$  and  $M1/E2$  multipolarity, respectively, to account for their relative intensities. With  $E1$  multipolarity for the 142-keV transition, the total conversion coefficient of the 337-keV  $\gamma$  ray is found, from intensity balance, to be  $\alpha_T = 0.68 \pm 0.36$ . Comparison with theoretical coefficients [38] ( $E1, 0.023$ ;  $M1, 0.313$ ;  $E2, 0.082$ ;  $M2, 1.08$ ; and  $E3, 0.392$ ) indicates this value is consistent with mixed  $M2/E3$  character for this 337-keV transition. Further, the observed branching ratios imply upper limits on the transition strength of the 337-keV transition of  $4.2 \times 10^{-3}$  Weisskopf, or single-particle, units (W.u.), for pure  $M2$  multipolarity and 32 W.u. if it is a pure  $E3$  transition. These strengths are acceptable but very difficult to reconcile with those of the  $\frac{29}{2}^-$  isomer in the heavier isotopes. In both  $^{191}\text{Pb}$  and  $^{193}\text{Pb}$ , the  $\frac{29}{2}^-$  isomer is the bandhead for a so-called shears band and is identified with the  $\pi(h_{9/2}i_{13/2})_{11-\nu}(i_{13/2})^{-1}$  configuration. In both cases, its lifetime is approximately 10 ns [21,30] and one of its main decays is an  $E1$  transition of about 150-keV [24,30] to a  $\frac{27}{2}^+$  level. Since the excitation energy of the yrast  $\frac{27}{2}^+$  level decreases in energy with decreasing  $A$  at about the same rate as that of the yrast  $\frac{29}{2}^-$  level, it is difficult to understand the absence of a corresponding  $\frac{27}{2}^+$  level in  $^{189}\text{Pb}$  to which a  $\frac{29}{2}^-$  level at 2435 keV could decay via an  $E1$  transition. The level at 2241 keV (Fig. 1) might be considered as a candidate for the  $\frac{27}{2}^+$  level; however, if this were so, the 194-keV  $E1$  transition strength would be about five orders of magnitude weaker than the corresponding transitions in  $^{191}\text{Pb}$  and  $^{193}\text{Pb}$ , and the observed ratio of the intensities of the 194- and 142-keV  $\gamma$  rays would be inconsistent with their implied multiplicities of  $E1$  and  $M1/E2$ , respectively.



On the other hand, if the  $\frac{33}{2}^+$  state were responsible for the 32- $\mu\text{s}$  lifetime, then, in view of the 337- and 609-keV decays to  $\frac{25}{2}^+$  states, the level at 2435 keV would have to be the  $\frac{29}{2}^+$  state of the same configuration, populated by an unobserved transition from the  $\frac{33}{2}^+$  state. If the energy of this transition was greater than 85 keV, it should have been present in the 819-keV coincidence gate (top panel of Fig. 6) with an intensity greater than about 10% of that of the 468-keV line. No candidate peak above 85 keV is observed, so if this transition exists, its energy is less than 85 keV and it may be obscured by the Pb x rays. If the 2435-keV level has  $J^\pi = \frac{29}{2}^+$ , the 337- and 609-keV transitions from this level would have  $E2$  multipolarity and the 142- and 194-keV transitions would probably be  $M1/E2$  admixtures. Assuming the 142-keV transition has pure  $M1$  multipolarity, intensity balances give  $\alpha_T = 0.30 \pm 0.30$  for the total conversion coefficient of the 337-keV  $\gamma$  ray, consistent with  $E2$  multipolarity. Consideration, in the following section, of transition strengths and likely configurations for the states concerned favors attributing the 32- $\mu\text{s}$  lifetime to the (unobserved)  $\frac{33}{2}^+$  state of the  $\nu(i_{13/2})^{-3}$  configuration and assigning  $J^\pi = \frac{29}{2}^+$  to the 2435-keV level, as shown in Fig. 1.

Note also that since the 337- and 609-keV transitions depopulate the same level at 2435 keV, the 2436-keV state deduced from the prompt decays must be a different level, despite the close similarity of their excitation energies; if they were the same, one would expect to see 337-keV  $\gamma$  rays in the prompt  $\gamma$ - $\gamma$  coincidence data (Fig. 4), and no such line was observed.

#### IV. DISCUSSION

While some of the deductions leading to the level scheme of Fig. 1 are based on comparisons with neighboring odd-mass isotopes and isotones as well as on plausibility arguments, it is possible, by further appeal to such comparisons, to gain information on the structures that dominate the high-spin states of  $^{189}\text{Pb}$ .

The yrast sequence  $\frac{13}{2}^+$ ,  $\frac{17}{2}^+$  (819 keV),  $\frac{21}{2}^+$  (1287 keV), and  $\frac{25}{2}^+$  (1825 keV) can be identified with the members of the  $\nu(i_{13/2})^{-3}$  multiplet in the spherical minimum of the potential well, although there is probably some mixing with other neutron excitations such as the  $(h_{9/2})^{-2}(i_{13/2})^{-1}$  configuration. Similar sequences are prominent in the heavier, odd-mass lead isotopes where the  $\frac{29}{2}^+$  and the isomeric  $\frac{33}{2}^+$  members are also observed. As argued in the preceding section, it is possible that the  $\frac{33}{2}^+$  member, although not directly observed, is responsible for the 32- $\mu\text{s}$  lifetime in  $^{189}\text{Pb}$  and that the 2435-keV level corresponds to the  $\frac{29}{2}^+$  member of this multiplet. If so, the  $\frac{33}{2}^+$  to  $\frac{29}{2}^+$  transition energy is presumably less than 85 keV, and the strength of the  $E2$  transition between the two states would be less than  $10^{-2}$  W.u. for all energies between 85 and 20 keV. This may be compared with the values 0.43 and 1.0 W.u. that have been measured [21,30] for the strengths of the corresponding transition in  $^{191}\text{Pb}$  and  $^{193}\text{Pb}$ , respectively.

To a good approximation, the  $\frac{33}{2}^+$  and  $\frac{29}{2}^+$  states in question in  $^{189}\text{Pb}$  should both arise from a configuration with seven neutrons in the  $i_{13/2}$  subshell and seniority  $\nu = 3$ . According to this model, the  $E2$  transition probability  $B(E2; \frac{33}{2}^+ \rightarrow \frac{29}{2}^+)$  should vanish for  $^{189}\text{Pb}$  (the so-called midshell cancellation [39]). The very small value implied by the data ( $< 0.01$  W.u.) is consistent with this expectation; the nonzero value can be attributed to small contributions from other configurations to the wave functions of the states involved.

If the 2435-keV level is the  $\frac{29}{2}^+$  member of the  $\nu(i_{13/2})^{-3}$  multiplet, then one would expect its main decay path to be via the 609-keV transition to the  $\frac{25}{2}^+$  member of the same configuration. The fact that the  $B(E2)$  for this transition is approximately 1% of that for the competing 337-keV transition can be understood qualitatively in terms of the same midshell cancellation that is expected to affect the  $\frac{33}{2}^+$  to  $\frac{29}{2}^+$  transition.

As discussed in the preceding section, the level at 638-keV excitation observed in the present work is identified with an excited  $\frac{13}{2}^+$  level at that excitation seen by Van de Vel *et al.* [20] in the  $\alpha$  decay of  $^{193}\text{Po}$ . Based mainly upon the similarity of the trend of the excitation energies of the excited  $\frac{13}{2}^+$  states in  $^{189-197}\text{Pb}$  to that of the oblate,  $0^+$ , intruder states in the even-mass neighbors, these authors interpret the excited  $\frac{13}{2}^+$  states as resulting from the coupling of an odd  $i_{13/2}$  neutron to the  $0^+$  bandhead of the oblate  $\pi(2p-2h)$  excitation in the even-mass core. They find that this interpretation is supported by potential-energy-surface calculations which predict an oblate minimum at a deformation of  $\beta_2 \approx 0.18$ ,  $\gamma \approx -60^\circ$ . In the present work, the excited  $\frac{13}{2}^+$  state at 638 keV is populated by a 504-keV  $\gamma$  ray from the second excited  $\frac{17}{2}^+$  state at 1142 keV. Although the latter state appears to be a member of a prolate band (see below), the presence of the 504-keV transition suggests a contribution to its wave function from the  $\frac{17}{2}^+$  member of a band built on the  $\frac{13}{2}^+$  oblate intruder.

The comparison in Fig. 8 of a sequence of levels and transitions in  $^{189}\text{Pb}$  with part of a rotational band in  $^{187}\text{Hg}$  reported by Hannachi *et al.* [32] and the accompanying discussion in Sec. III lead to the interpretation that the two reflect similar structures. The analysis of Hannachi *et al.* indicates that the  $^{187}\text{Hg}$  band is a strongly coupled structure built on the  $\frac{9}{2}^+$  [624] neutron orbital at prolate deformation ( $\beta_2 \sim 0.25$ ). There is, however, some signature splitting, indicating  $K$  mixing; so, following Lane *et al.* [40], we refer to it as a mixed  $i_{13/2}$  neutron band.

In Fig. 9, the excitation energies of the two level sequences, with the rotational energy  $9.6J(J+1)$  keV subtracted, are plotted against  $J(J+1)$ . Comparison of the two lends further support to the proposition that they have a common structural origin. They have similar moments of inertia, and signature splitting is present in both cases. The sign of the signature splitting in the low-spin region is the same, although the bands in  $^{189}\text{Pb}$  do not appear to show the change in sign seen in  $^{187}\text{Hg}$ . In any case, both bands may be distorted in the low-spin region by interference from other bands: the decoupled, oblate band in  $^{187}\text{Hg}$ ; and the yrast spherical states in  $^{189}\text{Pb}$ .

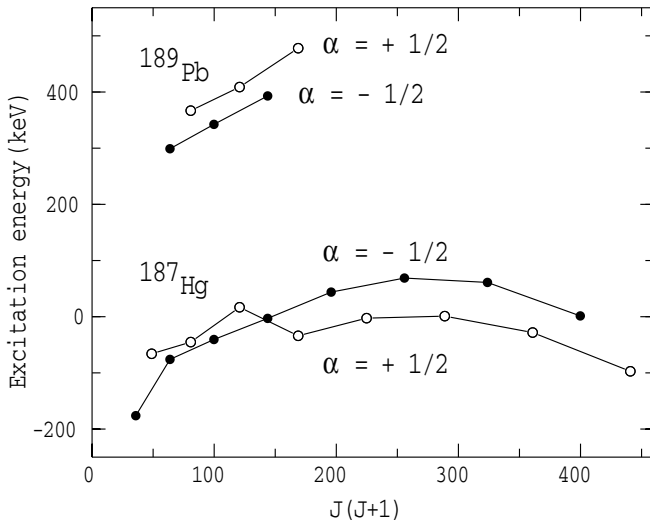


FIG. 9. Variation with  $J(J+1)$  of the excitation energies of prolate bands in  $^{187}\text{Hg}$  and  $^{189}\text{Pb}$ , after subtraction of the energies of a simple rotor. In each band, there are two sequences labeled by their signatures  $\alpha$ .

In both cases, the excitation energies are relative to a low-lying  $\frac{13}{2}^+$  isomer which, in  $^{187}\text{Hg}$ , is the bandhead of the oblate band, whereas, in  $^{189}\text{Pb}$ , it is the lowest such state in the spherical potential minimum. If, instead, the  $^{189}\text{Pb}$  energies were to be taken relative to the oblate  $\frac{13}{2}^+$  level at 638 keV, the  $^{189}\text{Pb}$  levels in Fig. 9 would fall about 250 keV below the  $^{187}\text{Hg}$  band. This suggests that the difference between the prolate and oblate potential minima in  $^{189}\text{Pb}$  is about 250 keV less than it is in  $^{187}\text{Hg}$ . This is probably due mostly to the influence of the additional pair of protons in  $^{189}\text{Pb}$  which, for oblate deformation, are likely to lead to a significantly higher energy for the oblate  $\frac{13}{2}^+$  state in this nucleus.

The indications of significant  $E0$  components (Table II) in the 272- and 324-keV transitions in  $^{187}\text{Pb}$  provide further support for the interpretation of the level scheme in terms of structures associated with different shapes. Such  $E0$  components can only occur (see, e.g., [41]) if the states concerned are mixed and have different deformations. The excitation energies are sufficiently close for significant mixing to be plausible and the evidence from systematics suggests that these two transitions are between structures in the prolate and spherical wells.

## V. CONCLUSION

To summarize, the present work reports a study, both in-beam and out-of-beam, of the high-spin states of  $^{189}\text{Pb}$ . The level scheme is dominated by a 32- $\mu\text{s}$  isomer from which there is a complex pattern of decay paths to a very-long-lived  $\frac{13}{2}^+$  isomer expected to lie about 100 keV above the low-spin ground state. The 32- $\mu\text{s}$  isomer is probably the  $\frac{33}{2}^+$  member of the  $\nu(i_{13/2})^{-3}$  multiplet although it is not directly observed. Comparison of the properties of the levels below the isomer with those of neighboring isotopes and isotones reveals evidence for three structures: yrast states arising primarily from the  $\nu(i_{13/2})^{-3}$  multiplet in the spherical potential minimum; an excited  $\frac{13}{2}^+$  level from the coupling of an odd  $i_{13/2}$  neutron to the oblate  $[\pi(2p-2h)]_{0+}$  state in the even-mass core; and a strongly coupled, mixed  $i_{13/2}$  neutron band at prolate deformation.

## ACKNOWLEDGMENTS

This work was supported in part by the Australian Government's Department of Industry, Science and Technology and by the U.S. Department of Energy, Office of Nuclear Physics, under Contract No. W-31-109-ENG-38.

- 
- [1] J. Heese *et al.*, Phys. Lett. **B302**, 390 (1993).  
 [2] A. M. Baxter *et al.*, Phys. Rev. C **48**, R2140 (1993).  
 [3] W. C. Ma *et al.*, Phys. Lett. **B167**, 277 (1986).  
 [4] J. K. Deng *et al.*, Phys. Rev. C **52**, 595 (1995).  
 [5] M. G. Porquet *et al.*, J. Phys. G **18**, L29 (1992).  
 [6] F. R. May, V. V. Pashkevich, and S. Frauendorf, Phys. Lett. **B68**, 113 (1977).  
 [7] R. Bengtsson and W. Nazarewicz, Z. Phys. A **334**, 269 (1989).  
 [8] W. Nazarewicz, Phys. Lett. **B305**, 195 (1993).  
 [9] A. N. Andreyev *et al.*, Nature **405**, 430 (2000).  
 [10] G. D. Dracoulis, A. P. Byrne, A. M. Baxter, P. M. Davidson, T. Kibedi, T. R. McGoram, R. A. Bark, and S. M. Mullins, Phys. Rev. C **60**, 014303 (1999).  
 [11] G. D. Dracoulis, G. J. Lane, A. P. Byrne, T. Kibedi, A. M. Baxter, A. O. Macchiavelli, P. Fallon, and R. M. Clark, Phys. Rev. C **69**, 054318 (2004).  
 [12] G. D. Dracoulis, A. P. Byrne, and A. M. Baxter, Phys. Lett. **B432**, 37 (1998).  
 [13] T. Duguet, M. Bender, P. Bonche, and P.-H. Heenen, Phys. Lett. **B559**, 201 (2003).  
 [14] R. Fossion, K. Heyde, G. Thiamova, and P. Van Isacker, Phys. Rev. C **67**, 024306 (2003).  
 [15] R. R. Rodríguez-Guzmán, J. L. Egido, and L. M. Robledo, Phys. Rev. C **69**, 054319 (2004).  
 [16] M. Bender, P. Bonche, T. Duguet, and P.-H. Heenen, Phys. Rev. C **69**, 064303 (2004).  
 [17] J. C. Griffin *et al.*, Nucl. Phys. **A530**, 401 (1991).  
 [18] J. Vanhorenbeeck *et al.*, Nucl. Phys. **A531**, 63 (1991).  
 [19] A. N. Andreyev *et al.*, Phys. Rev. C **66**, 014313 (2002).  
 [20] K. Van de Vel *et al.*, Phys. Rev. C **65**, 064301 (2002).  
 [21] J. M. Lagrange *et al.*, Nucl. Phys. **A530**, 437 (1991).  
 [22] J. R. Hughes *et al.*, Phys. Rev. C **51**, R447 (1995).

- [23] D. Roßbach *et al.*, Nucl. Phys. **A660**, 393 (1999).
- [24] G. Baldsiefen *et al.*, Phys. Rev. C **54**, 1106 (1996).
- [25] L. Ducroux *et al.*, Z. Phys. A **356**, 241 (1996).
- [26] S. Chmel, F. Brandolini, R.V. Ribas, G. Baldsiefen, A. Gorgen, M. DePoli, P. Pavan, and H. Hubel, Phys. Rev. Lett. **79**, 2002 (1997).
- [27] R. M. Clark and A. O. Macchiavelli, Annu. Rev. Nucl. Part. Sci. **50**, 1 (2000).
- [28] N. Fotiades *et al.*, Phys. Rev. C **57**, 1624 (1998).
- [29] J. M. Lagrange *et al.*, Nucl. Phys. **A648**, 64 (1999).
- [30] A. M. Baxter *et al.*, Phys. Rev. C (to be submitted).
- [31] A. M. Baxter *et al.*, Phys. Rev. C **58**, 2671 (1998).
- [32] F. Hannachi *et al.*, Nucl. Phys. **A481**, 135 (1988).
- [33] C. N. Davids and J. D. Larson, Nucl. Instrum. Methods Phys. Res. B **40/41**, 1224 (1989); C. N. Davids *et al.*, *ibid.* **70**, 358 (1992).
- [34] M.-G. Porquet *et al.*, Phys. Rev. C **44**, 2445 (1991); W. Reviol *et al.*, Phys. Scr. **T56**, 167 (1995).
- [35] M. Kaci *et al.*, Z. Phys. A **354**, 267 (1996).
- [36] G. Baldsiefen *et al.*, Nucl. Phys. **A587**, 562 (1995).
- [37] G. Baldsiefen *et al.*, Nucl. Phys. **A574**, 521 (1994).
- [38] I. M. Band *et al.*, At. Data Nucl. Data Tables **81**, 1 (2002).
- [39] R. D. Lawson, *Theory of the Nuclear Shell Model* (Clarendon, Oxford, 1980).
- [40] G. J. Lane *et al.*, Nucl. Phys. **A589**, 129 (1995).
- [41] K. Heyde and R. A. Meyer, Phys. Rev. C **42**, 790 (1990).